Paramagnetic-to-Diamagnetic Transition in Dense Liquid Iron and Its Influence on Electronic Transport Properties

Jean-Alexander Korell,[1] Martin French,[1] Gerd Steinle-Neumann,[2] and Ronald Redmer[1]
[1]*Universität Rostock, Institut für Physik, Albert-Einstein-Strasse 23-24, D-18059 Rostock, Germany*
[2]*Bayerisches Geoinstitut, Universität Bayreuth, D-95440 Bayreuth, Germany*

(Received 3 August 2018; revised manuscript received 21 December 2018; published 1 March 2019)

The electrical σ and thermal conductivity λ of liquid iron are calculated with spin-polarized density-functional-theory-based simulations over a significant pressure and temperature range using the Kubo-Greenwood formalism. We show that a paramagnetic state is stable in the liquid up to high temperatures at ambient pressure and that the discrepancy between experimental results and spin-degenerate simulations for σ and λ of more than 30% are reduced to within 10% with lower values resulting from the spin-polarized simulations. Along the 3700 K isotherm, we explore the persistence of magnetic fluctuations toward high densities, and beyond 20–50 GPa the liquid becomes diamagnetic, which suggests the existence of a continuous paramagnetic-to-diamagnetic transition. This transition exerts a significant influence on the physical properties of liquid iron, especially on σ and λ, and is potentially of high relevance for dynamo processes in Mercury and Mars.

DOI: 10.1103/PhysRevLett.122.086601

The understanding of electrical transport properties of liquid metals has seen significant advances over the past decade as an increasing number of studies employed the Kubo-Greenwood formalism [1,2] on ionic configurations from density-functional-theory-based molecular dynamics (DFT-MD). This computational approach has successfully been applied to aluminum [1,3–6], lithium [7], sodium [8], molybdenum [9], copper [10,11], and iron [12,13].

Among those, the work on iron [12,13] and iron alloys [12,14,15] has been of great interest in geophysics, as their electrical (σ) and thermal conductivity (λ) play a significant role in assessing the efficiency of magnetic field generation and on the thermal evolution of Earth's core [16,17]. Calculations for σ of liquid Fe and Fe-Si alloys show good agreement with measurements from shock wave experiments at pressures $p > 100$ GPa [18,19] and some static experiments in the diamond anvil cell [20,21]. At lower and especially at ambient pressure, Kubo-Greenwood values for σ are significantly larger than experimental data [22–27]. This discrepancy can partly be attributed to the underlying equation of state from the DFT-MD simulations that underestimates molar volumes at ambient pressure by as much as 20% [15,28]. But even if evaluated at the correct density ρ for ambient p, the difference in σ persists.

None of the DFT-MD or Kubo-Greenwood calculations mentioned in the previous paragraph have considered spin polarization, whereas a spin Hamiltonian model predicts disordered local moments in Fe stabilized by entropy to well above the melting temperature (T_M) [29]. This model even suggests that such a paramagnetic state persists to Earth's core conditions. The presence of local moments gives rise to a spin-disordered resistivity contribution, which was computed to be in the range of 100 $\mu\Omega$ cm at ambient pressure above the Curie temperature [30] and 20 $\mu\Omega$ cm at conditions of Earth's core for bcc iron [31]. Two observations are worth pointing out: (i) Resistivity contributions due to electron-phonon scattering and spin disorder are not additive [31]; i.e., Matthiessen's rule does not apply, although it has been used in the analysis of resistivity data [32,33]; (ii) at ambient conditions, the computed spin-disorder resistivity [30] reaches values similar to the total measured resistivity [22].

Here we consider the influence of magnetism on electrical conductivity for liquid Fe directly in DFT-MD and linear response calculations for the Onsager coefficients within the Kubo-Greenwood formalism: We account for collinear magnetism in the electronic structure and, consequently, ionic configurations, using spin-polarized DFT. As Ruban, Belonoshko, and Skorodumova [29] have shown for bcc iron at ambient p, the magnetic moments resulting from such an approach are very similar to the disordered local moments from the effective Hamiltonian. We examine the influence of magnetism on both aspects of the simulations separately, i.e., DFT-MD and the Kubo-Greenwood calculations, to investigate their relative importance and assess differences to the previously published results on liquid Fe.

The molecular dynamics (MD) simulations use forces derived from finite-temperature (FT) DFT [34,35], on the basis of the Born-Oppenheimer approximation. The FT-DFT electronic structure calculations are performed within a collinear formulation of spin states [36,37] and employ the Perdew-Burke-Ernzerhof (PBE) [38] formulation for a semilocal generalized gradient (GGA) corrected exchange

correlation functional. Simulations are performed with the Vienna *ab initio* simulation package (VASP) 5.4.1 [39–41], using the projector augmented wave (PAW) method and the potential file [42,43] provided with VASP ($[\mathrm{Ar}]4s^2 3p^6$ valence configuration, labeled PAW_PBE Fe_GW) for the electron-core interaction. The plane-wave basis set is expanded to a cutoff energy E_{cut} of 1200 eV, and electronic states are calculated at the Baldereschi mean-value point [44]. The cubic cell is set up containing 70 atoms with periodic boundary conditions. With a Nosé-Hoover thermostat [45,46], we generate a canonical ensemble in which we run 2000–5000 time steps with a length of 2 fs after equilibration. All choices for numerical parameters (potential, E_{cut}, particle number, reciprocal space sampling, time steps, and total duration) are similar to those from previous studies for liquid iron [12,13] and were confirmed to be adequate by several test calculations with more stringent settings.

The electronic transport properties are subsequently computed using linear response theory (LRT) on the Kohn-Sham states [2]. Respective formulas for σ and λ are given in Supplemental Material [47], which includes Refs. [48–51]. These formulas are evaluated using ionic configurations from the MD simulations, averaged over 20–50 uncorrelated configurations per MD run. Numerical parameters for these static FT-DFT calculations are checked as well and were chosen identical to those from the MD simulations except for E_{cut}, which is reduced to 400 eV. At least 5 eV of bands with negligible occupation numbers were taken into account. The broadening parameter of the delta function was set to $\approx$0.005 eV. Calculations are performed consistently either spin polarized or spin degenerate for both MD and LRT, unless explicitly noted otherwise. The accuracy of our calculated values is 1%–2% for σ and 1%–4% for λ. Consequently, the Lorenz number L [47] is calculated with an accuracy of about 2%–6%. Supplemental Material [47] contains a table with our numerical results.

The total magnetic moment in the simulation cell of the DFT-MD simulations fluctuates around zero, characteristic for a paramagnetic state in the absence of an external field. The magnitude of fluctuations, illustrated by the square of the individual magnetic moments (Fig. 1), decreases systematically with both ρ and T. The most prominent effect due to the presence of magnetic fluctuations in liquid iron is therefore expected at low ρ and low T.

Local magnetic moments in the paramagnetic state can affect conductivity in both parts of the computational approach, i.e., DFT-MD and LRT. We consider the respective influences by a direct comparison of spin-polarized and spin-degenerate calculations at $\rho = 6.75$ g/cm^3 and $T = 2250$ K (Fig. 2).

The pair correlation function $g(r)$ of the spin-polarized DFT-MD configurations reveals a slight shift of interatomic distances to larger values and more pronounced maxima and minima. The nearest neighbor distance, measured as the first maximum in $g(r)$, is shifted by 0.08 Å for the spin-polarized results relative to the spin-degenerate simulations (2.47 Å), which is also reflected by a higher pressure (magnetic p) calculated for the spin-polarized case (Fig. 3).

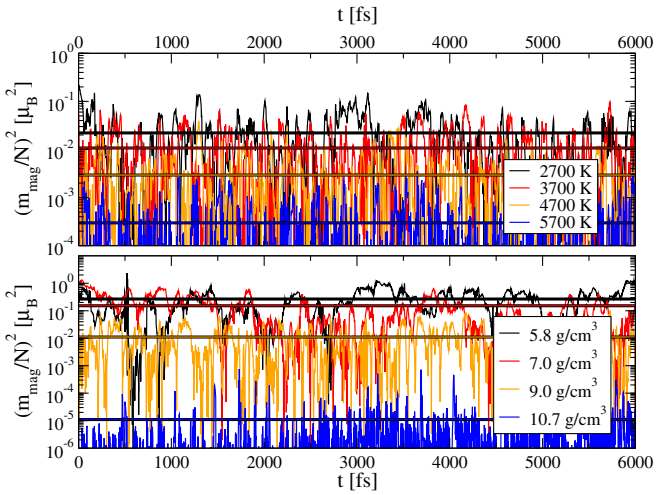

FIG. 1. Quadratic magnetic moment per atom at $\rho = 9$ g/cm^3 as a function of the simulation time for different T (upper panel) and at $T = 3700$ K for different ρ (lower panel). Horizontal lines show time averages of the moment squares.

In the LRT, spin polarization influences the electron velocity matrix elements that enter the calculation of the Onsager coefficients [2,47] and enforces a spin selection rule to take effect, due to the difference in electronic structure of the spin-up and spin-down states. Figure 2 shows the dynamic electrical conductivity calculated with

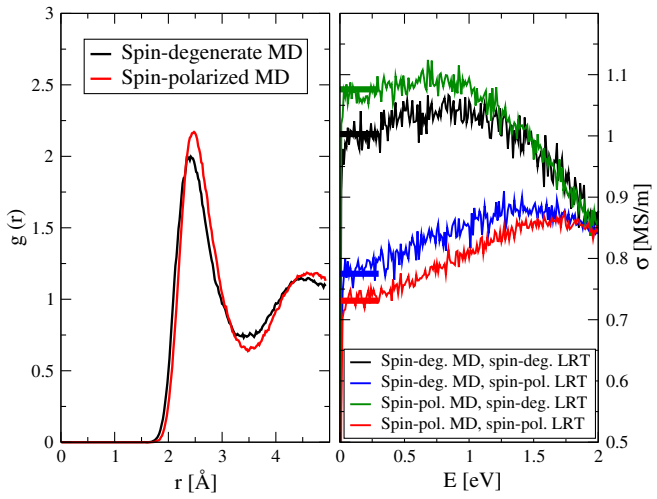

FIG. 2. Pair correlation function from a spin-degenerate and a spin-polarized DFT-MD simulation at $\rho = 6.75$ g/cm^3 and $T = 2250$ K (left panel). Frequency-dependent electrical conductivity derived at the same thermodynamic state using all four possible combinations of spin-polarized and spin-degenerate MD and LRT (right panel). dc values are indicated by thick bars of the same color.

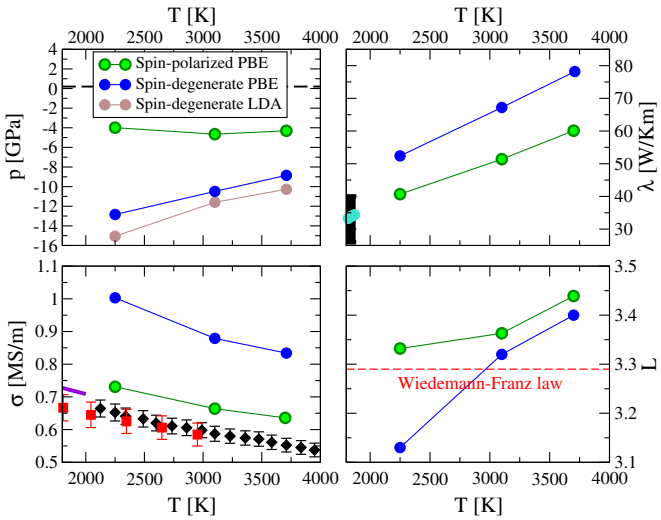

FIG. 3. Pressure and transport properties at densities and temperatures from exploding wire experiments [24]. The results from our work are represented as indicated in the legend. The thin dashed line in the upper left panel indicates the experimental pressure of 0.2 GPa [24]. Measurements of the electrical conductivity by Hixson, Winkler, and Hodgdon [24], Beutl, Pottlacher, and Jäger [25], and van Zytveld [22] are shown as diamonds, squares, and a purple line, respectively. Experimental thermal conductivities reported by Mills, Monaghan, and Keene [52] and Nishi *et al.* [53] are indicated in black and turquoise, respectively.

all four combinations of the spin-degenerate and spin-polarized approach for DFT-MD and LRT.

This comparison illustrates that the influence of spin polarization on optical conductivity through LRT is larger than that of structural changes from DFT-MD simulations. Regardless of whether the spin-polarized LRT calculations are based on configurations from spin-polarized or spin-degenerate MD simulations, zero-frequency values for σ are in the range of 0.7–0.8 MS/m, while spin-degenerate LRT yields values that exceed 1.0 MS/m.

Direct dc measurements of electrical resistivity of liquid Fe at ambient pressure with high precision are limited to 2300 K [22], and measurements at higher T require dynamic techniques [24,25]. These are exploding wire experiments that generate isobaric states (e.g., at 0.2 GPa [24]) and allow for direct measurements of ρ and T. To compare to the experimental data, we perform simulations at densities and temperatures measured in the experiments of Hixson, Winkler, and Hodgdon [24], with $\rho = 6.75$, 6.15, and 5.80 g/cm^3 at $T = 2250$, 3100, and 3710 K, respectively. It is worth pointing out that differences in the density between the two exploding wire studies [24,25] exceed 0.1 g/cm^3 at 3000 K and that the densities of Hixson, Winkler, and Hodgdon [24] are in closer agreement with the thermodynamic model by Komabayashi [54].

In the spin-degenerate PBE simulations, pressure from experiments is underestimated by 8–13 GPa, with the p difference decreasing with T (Fig. 3). Using the local-density approximation (LDA) to exchange and correlation leads to an additional pressure difference of 1–2 GPa. While for most nonmagnetic materials, including transition metals, LDA is known to overbind and PBE to underbind [55,56], for Fe both the LDA and GGA predict volumes that are too low for the crystalline phases [57]. Spin-polarized results, by contrast, show a significantly reduced pressure deviation of about −4 GPa that is T independent, thus correcting the failure of spin-degenerate simulations to a large extent. This behavior is in much better agreement with LDA and PBE calculations for several nonmagnetic materials that show differences in p due to the approximate exchange and correlation functionals to remain largely T independent until at least the critical point [58].

Electrical conductivity values from the spin-degenerate PBE calculations decrease with T at a higher rate and are larger by ≈30% than experimental values [22,24,25]. When spin polarization is taken into account, differences decrease to ≈10% (Fig. 3), and the T dependence becomes similar to the experimental one.

The thermal conductivity of liquid iron has been measured [52,53] only slightly above $T_M = 1808$ K [22], and significant differences exist between experiments [52]. Although we cannot equilibrate liquid states very close to the melting point in the DFT-MD simulations due to restrictions in the system size, the predicted thermal conductivity from our calculations behaves almost linearly with T along the experimental isobar and allows for a reasonable extrapolation to T_M (Fig. 3); for the spin-polarized results, the extrapolation falls within the range of experimental data. Thermal conductivity values from spin-degenerate calculations are significantly higher, and an extrapolation to T_M overshoots experimental values. The Lorenz numbers L of both spin-degenerate and spin-polarized simulations fulfill the Wiedemann-Franz law within 5% of the Drude-Sommerfeld value of $\pi^2/3$. A slight increase in L with T is similar to earlier DFT-MD results for dense hydrogen plasmas [2].

As illustrated in Fig. 1, magnetic fluctuations decrease with compression, and the differences in both the equation-of-state and transport properties are expected to vanish at high densities. As we have seen (Fig. 3), the p difference is ≈4.3 GPa at ambient volume; this difference decreases along with the magnetic fluctuations, and at $\rho = 9.0$ g/cm^3 (with magnetic fluctuations below 10^{-2} μ_B^2) the p difference has disappeared (Fig. 4). This behavior resembles predictions of the loss of magnetism in hexagonal close packed (hcp) iron in an antiferromagnetic (AFM) structure at high pressure that has been set up to model local spin fluctuations [59]. Our simulations show that the magnetic fluctuations drop most significantly in the ρ range between 8 and 9 g/cm^3 from 0.15 to 0.033 μ_B^2, yet smoothly and without a critical loss of magnetism as predicted for other transition metals, e.g., Co [60,61]. Interestingly, the p range

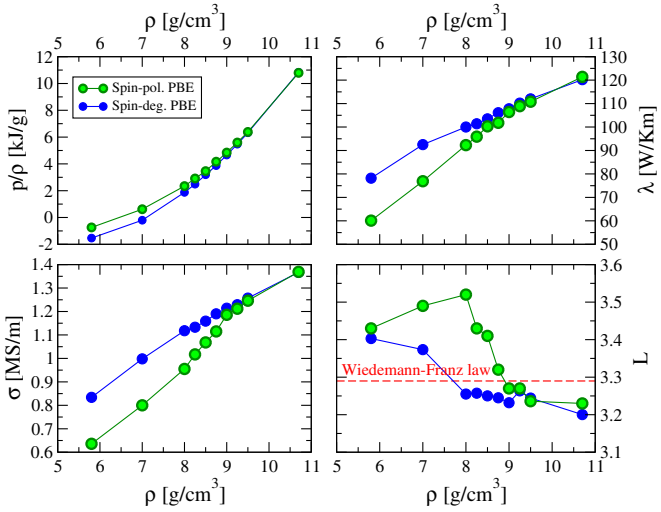

FIG. 4. Reduced pressure p/ρ and electronic transport properties as a function of densities along a 3700 K isotherm. Results from the current work (spin polarized and spin degenerate) are represented as indicated in the legend.

for the most significant decay of magnetic fluctuations (20–50 GPa) coincides with the loss of magnetism predicted in the AFM structure of hcp iron [59].

The electrical conductivity of the spin-degenerate calculations follows a smooth and simple trend (Fig. 4). The results from the spin-polarized calculations, however, display a well-pronounced increase in slope between 8 and 9 g/cm^3; at $\rho \geq 9.5$ g/cm^3, they become indistinguishable from the spin-degenerate results. A similar but less pronounced behavior occurs for the thermal conductivity. This indicates the presence of a continuous transition between paramagnetic and diamagnetic liquid states in the phase diagram of iron.

The Lorenz number of the spin-degenerate calculations decreases with ρ, and its deviation from the Wiedemann-Franz law changes from positive to negative, which occurs between 8 and 9 g/cm^3 (Fig. 4). At $\rho < 9$ g/cm^3, the L of the spin-polarized results is significantly higher than the spin-degenerate values and increases with ρ. However, deviations from the Wiedemann-Franz law do not exceed 8%.

In summary, we have shown that considering spin polarization accounts for much of the discrepancy in electrical and thermal conductivity between Kubo-Greenwood results based on DFT-MD and experiments at low p. This discrepancy has been a significant impediment in the acceptance of Kubo-Greenwood results in the high-pressure mineral physics and geophysics community, where they play a significant role in considerations of the geodynamo. Small differences to experimental values remain both for equation-of-state and transport properties, but these are within the typical range of deviations of DFT-derived properties using (semi)local approximations to the exchange and correlation functional [56,58]. A fully noncollinear treatment of magnetism could further decrease this discrepancy, but such calculations are extremely challenging to converge for disordered systems and beyond the scope of the current work.

The magnitude of magnetic fluctuations decreases with ρ and T. Along the 3700 K isotherm, a pronounced change in σ occurs in a range of $\rho = 8.0$–9.0 g/cm^3, indicating a continuous paramagnetic-to-diamagnetic transition in liquid iron. The ρ-T behavior of the magnetic fluctuations suggests that this transition has a negative slope in p-T space. With diamond anvil cell experiments, it has become possible to probe the relevant range $p = 20$–50 GPa even above the melting line [27], but higher precision in the measurements will be required to detect differences of the scale described here between spin-polarized and spin-degenerate results.

At the conditions of Earth's core, magnetic fluctuations no longer play a role, such that prior results using the Kubo-Greenwood formalism [12–14] are reproduced to within a few percent and serve as a reliable basis for geodynamic considerations [16,62]. For cores of the smaller terrestrial planets in the Solar System, Mercury and Mars, magnetic fluctuations may play a role, although alloying elements in their cores like sulfur or silicon [63,64] may influence their existence and magnitude. Because of the presence of additional scattering centers, conductivities are already reduced to different degrees depending on the nature of light elements incorporated [65]; additional magnetic contributions can potentially remedy two important existing contradictions in geophysics. (i) They may resolve contradictory inferences on the varying influence of different light elements on electrical conductivity in experiments [33] and computations [65]. (ii) Thermal conductivity at low p may be reduced to the degree that values become similar to those used previously in models that describe the thermal evolution and magnetic field generation in Mercury [66] and Mars [67]. This would render the "new core paradox" for the energy source of a dynamo, termed by Olson [17], for the smaller planets pointless. Nevertheless, powering Earth's dynamo with high thermal conductivity remains a challenge [62].

We thank Fabian Wagle for helpful discussions. This work was supported by the Deutsche Forschungsgemeinschaft (DFG) within the FOR 2440. The *ab initio* calculations were performed at the North-German Supercomputing Alliance (HLRN) facilities and at the IT and Media Center of the University of Rostock.

[1] M. P. Desjarlais, J. D. Kress, and L. A. Collins, Phys. Rev. E **66**, 025401 (2002).
[2] B. Holst, M. French, and R. Redmer, Phys. Rev. B **83**, 235120 (2011).
[3] V. Recoules and J. P. Crocombette, Phys. Rev. B **72**, 104202 (2005).

[4] V. Vlček, N. de Koker, and G. Steinle-Neumann, Phys. Rev. B **85**, 184201 (2012).
[5] D. V. Knyazev and P. R. Levashov, Comput. Mater. Sci. **79**, 817 (2013).
[6] B. B. L. Witte, P. Sperling, M. French, V. Recoules, S. H. Glenzer, and R. Redmer, Phys. Plasmas **25**, 056901 (2018).
[7] A. Kietzmann, R. Redmer, M. P. Desjarlais, and T. R. Mattsson, Phys. Rev. Lett. **101**, 070401 (2008).
[8] M. Pozzo, M. P. Desjarlais, and D. Alfe, Phys. Rev. B **84**, 054203 (2011).
[9] M. French and T. R. Mattsson, Phys. Rev. B **90**, 165113 (2014).
[10] K. R. Cochrane, R. W. Lemke, Z. Riford, and J. H. Carpenter, J. Appl. Phys. **119**, 105902 (2016).
[11] I. C. Ezenwa, R. A. Secco, W. Yong, M. Pozzo, and D. Alfè, J. Phys. Chem. Solids **110**, 386 (2017).
[12] N. de Koker, G. Steinle-Neumann, and V. Vlček, Proc. Natl. Acad. Sci. U.S.A. **109**, 4070 (2012).
[13] M. Pozzo, C. Davies, D. Gubbins, and D. Alfè, Nature (London) **485**, 355 (2012).
[14] M. Pozzo, C. Davies, D. Gubbins, and D. Alfè, Phys. Rev. B **87**, 014110 (2013).
[15] F. Wagle, G. Steinle-Neumann, and N. de Koker, Phys. Rev. B **97**, 094307 (2018).
[16] C. Davies, M. Pozzo, D. Gubbins, and D. Alfè, Nat. Geosci. **8**, 678 (2015).
[17] P. Olson, Science **342**, 431 (2013).
[18] R. N. Keeler, in *Physics of High Energy Density*, edited by P. Caldirola and H. Knoepel (Academic, New York, 1971), pp. 106–125.
[19] G. Matassov, Ph.D. thesis, University of California, 1977.
[20] H. Gomi, K. Ohta, K. Hirose, S. Labrosse, R. Caracas, M. J. Verstraete, and J. W. Hernlund, Phys. Earth Planet. Inter. **224**, 88 (2013).
[21] H. Gomi, K. Hirose, H. Akai, and Y. Fei, Earth Planet. Sci. Lett. **451**, 51 (2016).
[22] J. B. van Zytveld, J. Phys. Colloq. **41**, 503 (1980).
[23] R. A. Secco and H. H. Schlössin, J. Geophys. Res. **94**, 5887 (1989).
[24] R. S. Hixson, M. A. Winkler, and M. L. Hodgdon, Phys. Rev. B **42**, 6485 (1990).
[25] M. Beutl, G. Pottlacher, and H. Jäger, Int. J. Thermophys. **15**, 1323 (1994).
[26] S. Kiarasi and R. A. Secco, Phys. Status Solidi B **252**, 2034 (2015).
[27] K. Ohta, Y. Kuwayama, K. Hirose, K. Shimizu, and Y. Ohishi, Nature (London) **534**, 95 (2016).
[28] H. Ichikawa, T. Tsuchiya, and Y. Tange, J. Geophys. Res. B **119**, 240 (2014).
[29] A. V. Ruban, A. B. Belonoshko, and N. V. Skorodumova, Phys. Rev. B **87**, 014405 (2013).
[30] A. L. Wysocki, K. D. Belashchenko, J. P. Velev, and M. van Schilfgaarde, J. Appl. Phys. **101**, 09G506 (2007).
[31] V. Drchal, J. Kudrnovský, D. Wagenknecht, I. Turek, and S. Khmelevskyi, Phys. Rev. B **96**, 024432 (2017).
[32] R. Weiss and A. Marotta, J. Phys. Chem. Solids **9**, 302 (1959).
[33] S. Suehiro, K. Ohta, K. Hirose, G. Morard, and Y. Ohishi, Geophys. Res. Lett. **44**, 8254 (2017).
[34] W. Kohn and L. J. Sham, Phys. Rev. **140**, A1133 (1965).
[35] N. D. Mermin, Phys. Rev. **137**, A1441 (1965).
[36] U. von Barth and L. Hedin, J. Phys. C **5**, 1629 (1972).
[37] R. Zeller, in *Computational Nanoscience: Do It Yourself!*, NIC Series, Vol. 31, edited by J. Grotendorst, S. Blügel, and D. Marx (John von Neumann Institute for Computing, Jülich, 2006), p. 419.
[38] J. P. Perdew, K. Burke, and M. Ernzerhof, Phys. Rev. Lett. **77**, 3865 (1996).
[39] G. Kresse and J. Hafner, Phys. Rev. B **47**, 558 (1993).
[40] G. Kresse and J. Hafner, Phys. Rev. B **48**, 13115 (1993).
[41] G. Kresse and J. Furthmüller, Phys. Rev. B **54**, 11169 (1996).
[42] P. E. Blöchl, Phys. Rev. B **50**, 17953 (1994).
[43] G. Kresse and D. Joubert, Phys. Rev. B **59**, 1758 (1999).
[44] A. Baldereschi, Phys. Rev. B **7**, 5212 (1973).
[45] S. Nosé, J. Chem. Phys. **81**, 511 (1984).
[46] W. G. Hoover, Phys. Rev. A **31**, 1695 (1985).
[47] See Supplemental Material at http://link.aps.org/supplemental/10.1103/PhysRevLett.122.086601 for formulas evaluated in the LRT calculations and a table with the numerical values for σ and λ.
[48] R. Kubo, J. Phys. Soc. Jpn. **12**, 570 (1957).
[49] D. A. Greenwood, Proc. Phys. Soc. **71**, 585 (1958).
[50] M. Gajdoš, K. Hummer, G. Kresse, J. Furthmüller, and F. Bechstedt, Phys. Rev. B **73**, 045112 (2006).
[51] M. French and R. Redmer, Phys. Plasmas **24**, 092306 (2017).
[52] K. C. Mills, B. J. Monaghan, and B. J. Keene, Int. Mater. Rev. **41**, 209 (1996).
[53] T. Nishi, H. Shibata, Y. Waseda, and H. Ohta, Metall. Mater. Trans. A **34**, 2801 (2003).
[54] T. Komabayashi, J. Geophys. Res. B **119**, 4164 (2014).
[55] P. Haas, F. Tran, and P. Blaha, Phys. Rev. B **79**, 085104 (2009).
[56] P. Söderlind and D. A. Young, Computation **6**, 13 (2018).
[57] L. Stixrude, R. E. Cohen, and D. J. Singh, Phys. Rev. B **50**, 6442 (1994).
[58] M. French and T. R. Mattsson, J. Appl. Phys. **116**, 013510 (2014).
[59] G. Steinle-Neumann, R. E. Cohen, and L. Stixrude, J. Phys. Condens. Matter **16**, S1109 (2004).
[60] G. Steinle-Neumann, Phys. Rev. B **77**, 104109 (2008).
[61] D. Antonangeli, L. R. Benedetti, D. L. Farber, G. Steinle-Neumann, A.-l. Auzende, J. Badro, M. Hanfland, and M. Krisch, Appl. Phys. Lett. **92**, 111911 (2008).
[62] S. Labrosse, Phys. Earth Planet. Inter. **247**, 36 (2015).
[63] L. Nittler, N. Chabot, T. Grove, and P. Peplowski, arXiv:1712.02187.
[64] H. Y. McSween and S. M. McLennan, in *Treatise on Geochemistry*, 2nd ed., edited by H. D. Holland and K. K. Turekian (Elsevier, Oxford, 2014), pp. 251–300.
[65] F. Wagle, G. Steinle-Neumann, and N. de Koker, C. R. Geosci. (in press).
[66] U. R. Christensen, Nature (London) **444**, 1056 (2006).
[67] J. P. Williams and F. Nimmo, Geology **32**, 97 (2004).